Superconductivity in Pt Doped BaFe2As2

ARTICLE *in* JOURNAL OF THE PHYSICAL SOCIETY OF JAPAN · JUNE 2012

Impact Factor: 1.59 · DOI: 10.1143/JPSJ.81.064704

5 AUTHORS, INCLUDING:

Shoubao Zhang
Kyoto University
36 PUBLICATIONS **240** CITATIONS

SEE PROFILE

DOI: 10.1143/JPSJ.81.064704

Superconductivity in Pt Doped $BaFe_2As_2$

Yanfeng GUO[1*], Xia WANG[2,3], Jun LI[2,3], Shoubao ZHANG[1], Kazunari YAMAURA[2,3,4†], and Eiji TAKAYAMA-MUROMACHI[1,2,4]

[1]*International Center for Materials Nanoarchitectonics (MANA), National Institute for Materials Science, Tsukuba, Ibaraki 305-0044, Japan*
[2]*Department of Chemistry, Graduate School of Science, Hokkaido University, Sapporo 060-0810, Japan*
[3]*Superconducting Properties Unit, National Institute for Materials Science, Tsukuba, Ibaraki 305-0044, Japan*
[4]*JST, Transformative Research-Project on Iron Pnictides (TRIP), Tsukuba, Ibaraki 305-0044, Japan*

(Received January 19, 2012; accepted March 28, 2012; published online May 11, 2012)

A high-pressure method was used to systematically dope an antiferromagnetically metallic compound, $BaFe_2As_2$, with Pt, and the doped compounds were studied using X-ray diffraction, energy dispersive X-ray spectroscopy, and by measuring the electrical resistivity, magnetic susceptibility, and specific heat. This method significantly increased the Pt doping level for $BaFe_2As_2$, resulting in a revision of the phase diagram proposed for $BaFe_{2-x}Pt_xAs_2$. The Pt doped system showed a dome-like superconductivity region in the thermal phase diagram ($0.02 < x < 0.20$) with an optimal T_c of 24.2 K ($x = 0.08$), instead of the unusually wide superconductivity region found in early studies. Further doping beyond the optimal Pt concentration led to T_c continuously decreasing toward zero. The common superconducting feature of the 3*d* and 4*d* doped systems, $BaFe_{2-x}M_xAs_2$ (M = Co, Ni, Rh, or Pd), was confirmed for the 5*d* doped system, $BaFe_{2-x}Pt_xAs_2$, which suggested that the electron–phonon coupling was insignificant at the superconducting state.

KEYWORDS: superconductivity, $BaFe_2As_2$, impurity effects, high pressure synthesis, antiferromagnetic metals

1. Introduction

Iron pnictide superconductors attract great interest in the condensed-matter-physics community because they capable of exhibiting superconductivity at T_c as high as 55 K.[1,2] Doping compounds to a AFe_2As_2 host (A = Ba, Sr, Ca, or Eu) is of particular interest because carrier doping to cause superconductivity (SC) can be controlled in many ways and sizable single crystals can be obtained without much technical difficulty.[3] In fact, the experimental results of many independent studies are often consistent and contribute greatly to revealing the nature of the SC of iron pnictide. The host, thus, has been intensively investigated in various ways; $BaFe_2As_2$ is antiferromagnetic (AFM) below ~140 K,[4] with similar AFM features below ~210 K for $SrFe_2As_2$[5] and ~190 K for $EuFe_2As_2$.[6] It has been argued the AFM order is primarily the result of Fermi surface nesting between the hole pockets around Γ and the electron pockets around M.[7] It is also argued that this nesting can be disrupted by chemical doping or physical squeezing, which weakens the magnetic order. The SC actually appears where the magnetic order is weak or absent.[8]

The chemical doping to AFe_2As_2 has been realized using a variety of *d* elements such as Co, Ni, Ru, Rh, Pd, Ir, and Rb.[9–13] Rather than the conventional carrier injection picture, a recent theoretical study involving density functional calculations for $BaFe_{2-x}X_xAs_2$ (X = Co, Ni, Cu, or Zn)[14,15] suggested that the doping results in an electronic modification through amendment of the Fe_2As_2 layer. Although the doping plays a significant role in establishing the SC,[16] the doping features still need to be studied further. For example, although the spin excitation and orbital fluctuation caused by the doping are probably essential to the SC, their relationships to it remain quite vague.[17,18] There have been many theoretical suggestions about the role of the doping. Thus, the progress made in the experimental studies on doping hold the promise of revealing the entire nature of the SC. The 122-type series is a valuable subject to use to experimentally study the doping.

Chemical doping to the 122 compound has been conducted mostly with group VIII atoms.[9–13] Regarding the 3*d* and 4*d* atoms in the group, the doped $BaFe_2As_2$ shows fairly common electronic diagram features over the doping. However, the 5*d* atom Pt doped $BaFe_{2-x}Pt_xAs_2$ shows features that are very different from the common features for the 3*d* and 4*d* systems.[19,20] In the early studies on $BaFe_{2-x}Pt_xAs_2$, SC appears over a remarkably wide doping range from $x = 0.02$–0.50 (25 atomic mole %), with an almost invariable T_c of ~25 K.[20] In addition, an Ir doping study revealed that T_c was almost invariable at ~24.2 K.[12,21] Note that among the 5*d* metals, only Pt[19,20] and Ir[12,21] were successful at turning on the SC in the 122 compounds AFe_2As_2. However, it might be possible that the early results were somewhat complicated by an inhomogeneous distribution of Pt or Ir. Thus, a well controlled Pt or Ir doping is required to draw a much more solid picture of the SC of the 5*d* element doped 122 system. The expected results at least provide us with useful information about electron–phonon coupling in the SC state because the atomic masses are entirely different.

In this study, crystals of $BaFe_{2-x}Pt_xAs_2$ ($x = 0$–0.25) were grown under high-pressure (HP) conditions, and the SC was investigated using electrical resistivity, magnetization, and specific heat measurements. The Pt distribution was certainly improved by employing the HP method. The results of this study significantly revised the earlier superconducting phase diagram proposed for $BaFe_{2-x}Pt_xAs_2$. It was confirmed that the common doping features for the 3*d* and 4*d* doped $BaFe_2As_2$ were valid even for the 5*d* doped system, which suggested that electron–phonon coupling in the SC state was insignificant.

*E-mail: guo.yanfeng@nims.go.jp
†E-mail: yamaura.kazunari@nims.go.jp

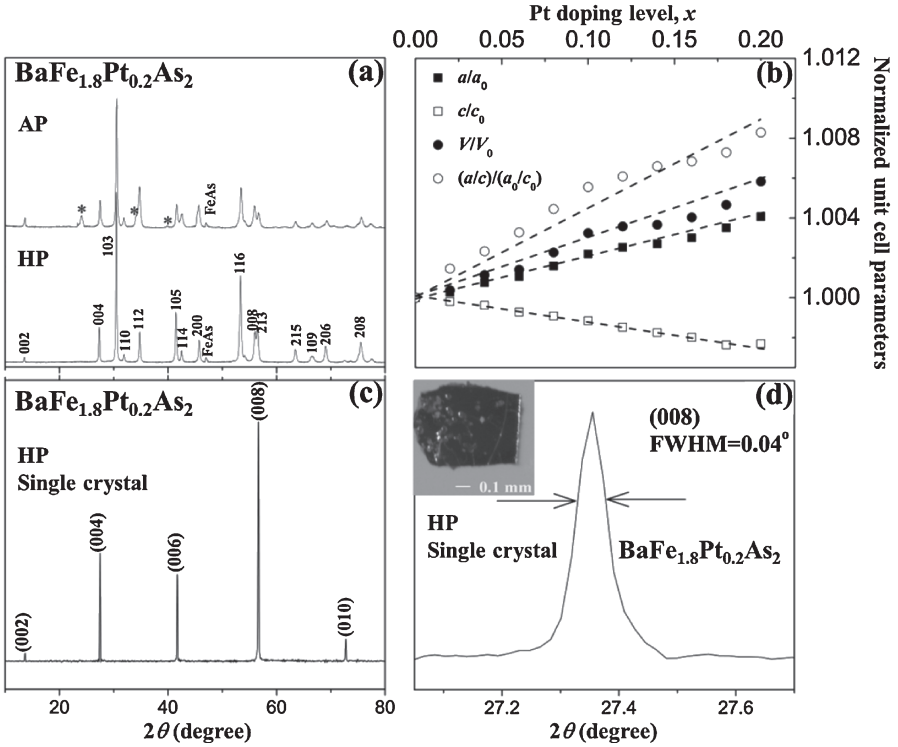

Fig. 1. (a) XRD patterns of polycrystalline $BaFe_{1.8}Pt_{0.2}As_2$ prepared using HP and AP methods. (b) Normalized unit cell parameters of the HP-prepared $BaFe_{1-x}Pt_xAs_2$, where $a_0 = 3.955(1)$ Å, $c_0 = 12.95(1)$ Å, and $V_0 = 202.6(3)$ Å^3 ($x = 0$). (c) XRD profile of a surface of a single crystal $BaFe_{1.8}Pt_{0.2}As_2$ (HP). (d) Photograph of a single crystal $BaFe_{1.8}Pt_{0.2}As_2$ (HP) having the approximate dimensions of $\sim 0.6 \times 0.5 \times 0.02\,mm^3$, and the FWHM of the (008) peak.

2. Experimental

Polycrystalline $BaFe_{2-x}Pt_xAs_2$ ($x = 0$, 0.04, 0.06, 0.08, 0.14, 0.16, 0.18, 0.20, and 0.25) was prepared as follows: binary precursors, BaAs and FeAs, were prepared from Ba pieces (scratched from a rod, 99.9%, Nilaco), Fe powder (100 mesh 99.9%, Rare Metallic), and As powder (99.999%, High Purity Chem.). Each mixture was placed in an evacuated quartz tube and heated at 700 °C for 10 h. Thereafter, a stoichiometric mixture of BaAs, FeAs, Fe, and Pt (99.9%, High Purity Chem.) was placed in a boron nitride cell. The nitride cell was sealed in a Ta capsule and then heated at 1300 °C for 2 h in a belt-type HP apparatus, which maintained a constant applied pressure at 3 GPa during the heating. The Ta capsule was quenched to room temperature before releasing the pressure. For a reference, selected mixtures of $BaFe_{2-x}Pt_xAs_2$ ($x = 0$, 0.10, and 0.20) were synthesized without applying the pressure (at ambient pressure, AP). Each mixture was placed in an evacuated quartz tube and heated at 1100 °C for a total of 40 h with several intermediate grindings to secure a homogeneous reaction. Selected single crystals at $x = 0.04$, 0.08, and 0.20 were grown under the HP condition using a self-flux method (6 h heating) with an additional 2 h of cooling to 1100 °C.

Phase identification by powder x-ray diffraction (XRD) was conducted at room temperature in a Rigaku diffractometer using Cu Kα radiation from 5–100° in 2θ. The lattice parameters of the phases were refined using the software Powder X.[22] True Pt and Fe compositions were investigated using energy dispersive X-ray spectroscopy (EDX), and the Pt distribution over a pellet was studied using a scanning electron microscope (SEM), Inca Energy 300 (Oxford Instruments).

The electrical resistivity, ρ, and specific heat, C_p, were measured using a physical properties measurement system from Quantum Design. Electrical contacts were prepared from silver epoxy and Au wires at four locations on a pellet for an electrical gauge current of 2 mA. The value of ρ was measured in a fixed magnetic field of 70 kOe or lower. C_p was measured using a time-relaxation method between 2 and 300 K in the apparatus. The magnetic susceptibility, χ, and isothermal magnetization (M) were measured using a magnetic property measurement system from Quantum Design. Loosely gathered powder was cooled to 2 K without applying a magnetic field, followed by warming to 300 K in an applied magnetic field of 10 or 0.01 kOe (zero-field cooling; ZFC). The sample was again cooled to 2 K in the field (field cooling; FC). M was measured in the apparatus at 2, 5, 8, 12, 15, and 18 K in a field range of $\pm$70 kOe.

3. Results and Discussion

XRD patterns of the polycrystalline $BaFe_{1.8}Pt_{0.2}As_2$ prepared under the HP and AP conditions are shown in Fig. 1(a). For the HP sample, the Bragg reflections were indexed very well using the $ThCr_2Si_2$-type structure model (space group: $I4/mmm$),[23] with the exception of tiny peaks for FeAs as an impurity. The pattern for the AP sample shows additional small Bragg peaks, which indicate the formation of $PtAs_2$ as an additional impurity. The $PtAs_2$ peaks were found to grow with an increase in the doping level. The size of the tetragonal unit cell of the HP sample changed almost linearly against the Pt content [Fig. 1(b)], suggesting that the doped Pt does go into the crystal structure, at least for $x \leq 0.20$. Because the Pt substitution for Fe may be isovalent[15] and the ionic size of Pt^{2+} is almost

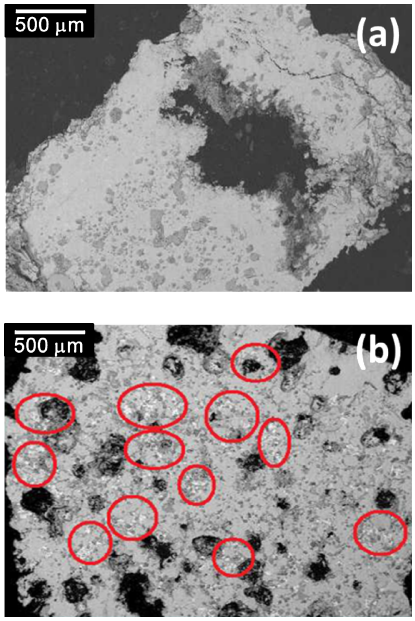

Fig. 2. (Color online) SEM images of polycrystalline $BaFe_{1.8}Pt_{0.2}As_2$ prepared using (a) HP and (b) AP methods. The HP sample shows a rather homogenous Pt distribution, while the AP sample shows many $PtAs_2$-rich clusters, as marked by small circles and ellipses.

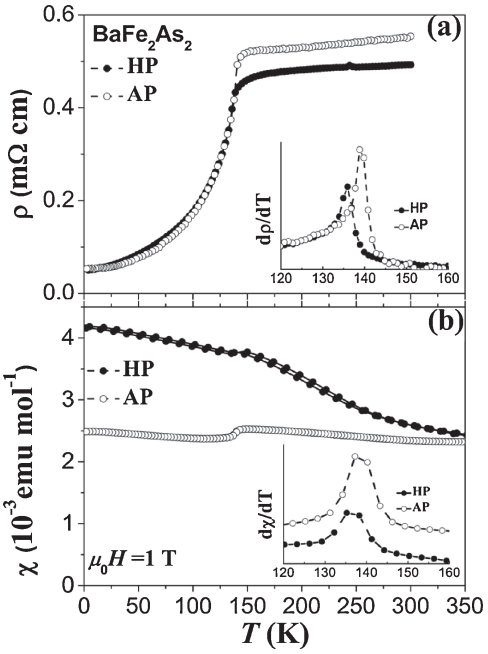

Fig. 3. T dependence of ρ of non-doped polycrystalline host $BaFe_2As_2$ prepared using (a) HP and (b) AP methods ($H = 10$ kOe). The $d\rho/dT$ and $d\chi/dT$ curves are plotted against T inside the figures.

comparable to that of Fe^{2+}, the unit cell change was expected to be very small. The result apparently coincides with this expectation. Although the substitution decreased the distance between the layers along the c-axis, it increased the average distance between the Fe atoms along the a-axis, which reflected different intra- and inter-plane bonding natures. The observed anisotropy was qualitatively comparable to what was observed for the Co, Ni, or other d element doped 122-type compounds, suggesting that the role of Pt in the doping is not far from that of the other d elements.

To further investigate the Pt doping, the composition was analyzed using EDX. Ten pieces of each of the selected HP samples ($x = 0.06$, 0.10, 0.14, 0.20, and 0.25) were measured, and the averaged Fe to Pt composition ratios were estimated to be 1.944/0.059 ($x = 0.06$), 1.897/0.102 (0.10), 1.856/0.144 (0.14), 1.804/0.206 (0.20), and 1.744/0.242 (0.25). The true Pt composition was in good accord with the starting composition, x, within one standard deviation. The result again confirmed the incorporation of Pt in the lattice.

The XRD pattern of the surface of a $BaFe_{1.8}Pt_{0.2}As_2$ crystal is shown in Fig. 1(c). Sharp peaks (002n, where n is an integer), with nothing else visible in the XRD pattern, indicated the crystal direction. The c-axis of the unit cell should be perpendicular to the surface. The full width at half maximum (FWHM) of the rocking curve of the main diffraction (008) was very sharp. It was 0.04°, as shown in Fig. 1(d), which suggests a good crystallization. A photograph of the crystal is shown in the inset of Fig. 1(d). The crystal size was approximately $0.6 \times 0.5 \times 0.02\,mm^3$.

The T_c of iron-based superconductors is argued to tightly correlate with the degree of distortion of the $FeAs_4$ tetrahedron; the As–Fe–As bond angle of the optimal T_c superconductors is close to the angle of the regular tetrahedron (109.5°).[24,25] Alternatively, the $(a/c)/(a_0/c_0)$ ratio is close to 1.005.[26] To investigate the lattice feature of the present Pt doped superconductor, the $(a/c)/(a_0/c_0)$ ratio is plotted against the Pt content in Fig. 1(b), which clearly shows a linear change. The optimal T_c of the present superconductor is observed at an x of 0.08–0.10 (shown later), where the ratio is fairly close to 1.005. Hence, the present result supports the argument.

SEM images of both the HP and AP prepared pellets of $BaFe_{1.8}Pt_{0.2}As_2$ are compared in Figs. 2(a) and 2(b), demonstrating contrasting Pt distributions. In the HP pellet, the Pt is almost homogenously distributed on this scale, while it is rather imperfectly distributed in the AP pellet. The region marked by ellipses and circles indicates a Pt rich area caused by the $PtAs_2$ impurity. This observation is consistent with what was suggested by the XRD study. The SEM observation supports the successful Pt doping up to an x of 0.20 under the HP condition.

Figure 3(a) shows $\rho(T)$ curves for both the AP and HP $BaFe_2As_2$ pellets measured in a zero magnetic field. The anomalous drop at ~150 K is suggestive of a correlation with a spin-density wave (SDW) or a structure transition, as observed in early studies.[4] The characteristic temperature (T_D) was 142 and 144 K for the HP and AP pellets, respectively, based on a $d\rho/dT$ analysis [inset for Fig. 3(a)]. T_D is fairly comparable with the temperatures reported previously,[4] indicating that the present result is not very different from the earlier results. The data confirm that there was little difference in ρ between the HP and AP samples (even the residual resistivity ratio, RRR, remains almost comparable). Figure 3(b) shows $\chi(T)$ curves for both samples. A comparable anomaly, which is presumably associated with the SDW, is detected: the $d\chi/dT$ analysis indicates peaks at 144 and 145 K for the HP and AP samples, respectively, which are fairly close to T_D by ρ. The small gap between the T_D values of the HP and AP samples might have been caused by the small degree of As non-stoichiometry.

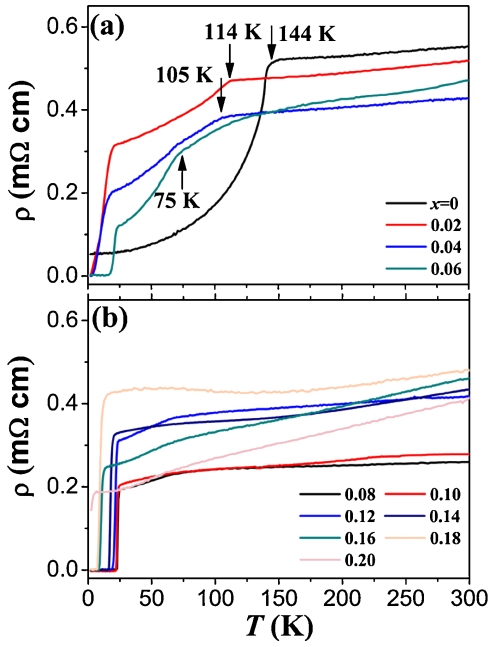

Fig. 4. (Color online) ρ vs T for polycrystalline $BaFe_{2-x}Pt_xAs_2$ (HP) for (a) $x = 0$–0.06 and (b) $x = 0.08$–0.20.

Figure 4 shows $\rho(T)$ curves for the pellets of $BaFe_{2-x}Pt_xAs_2$ ($x \leq 0.20$) prepared under the HP condition. A clear decrease in T_D with increasing Pt content is observed up to approximately $x = 0.08$ [Fig. 4(a)], while the room temperature ρ remains almost constant. In addition to T_D, another independent drop likely caused by the superconductivity appears at a much lower temperature ($T <$ 25 K). The T_c evolution is seen in Fig. 4(b); T_c rises to 24.2 K at $x = 0.08$ with a transition width of less than 1.5 K. For the further analysis of the superconducting transition, the x dependences of χ and ρ are plotted in Figs. 5(a)–5(j). At the lowest Pt content, the sample shows a weak diamagnetic signal at $T < 10$ K (the shielding fraction at 2 K is 14% of the full superconducting fraction). The fraction increased with increasing Pt content, and the largest fractions of 79–92% were observed at $x = 0.08$–0.14. Further Pt doping decreased the fraction, as well as T_c. The highest T_c by χ was 23.9 K ($x = 0.08$), which is comparable to the T_c by ρ.

For further investigation, C_p was measured between 2 and 300 K over the entire range of HP-synthesized polycrystalline pellets of $BaFe_{2-x}Pt_xAs_2$ ($0 \leq x \leq 0.20$). The Pt concentration dependence of C_p vs T is plotted in Fig. 6(a). The room temperature C_p values are almost x independent at 130–135 $J\,mol^{-1}\,K^{-1}$), approaching the Dulong–Petit limit [$n_{atom} \times 3R = \sim 125\,J\,mol^{-1}\,K^{-1}$, where R is the molar gas constant and n_{atom} is the number of atoms per mole]. A sharp peak is observed between 100 and 140 K, depending on x, which is likely the result of losing entropy during the SDW transition.[27] To see the peak clearly, an expanded C_p/T vs T plot is provided in the inset of Fig. 6(a); the peak gradually shifts toward the lower temperature with increasing x. The peak top position is ~135.4, 115.9, and 109.7 K at $x = 0$, 0.02, and 0.04, respectively. The Pt concentration dependence was almost consistent with the SDW transition found in the ρ and χ measurements. Unfortunately, the peak became broader and smaller with further Pt doping ($x \geq 0.06$) and disappeared or was masked by the lattice contribution (C_{latt}).

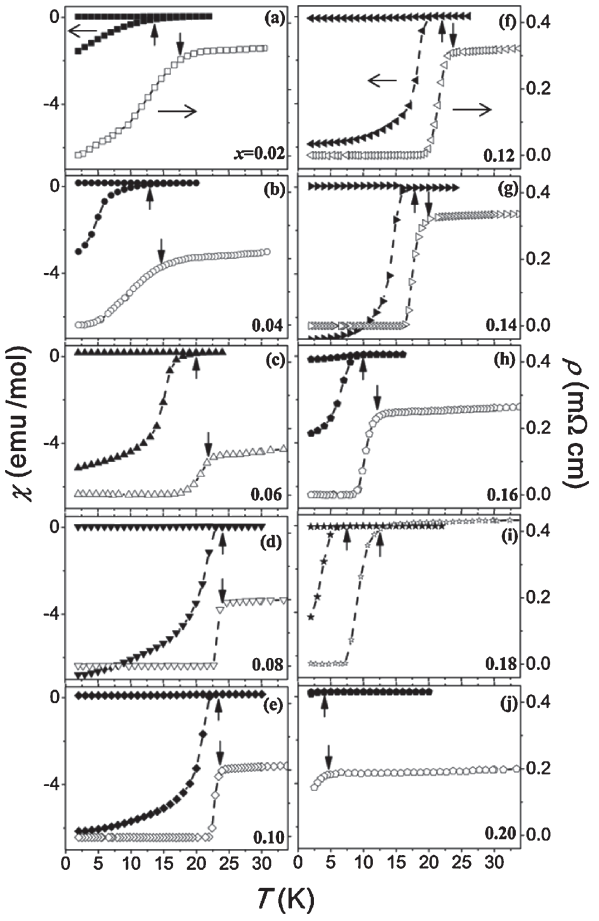

Fig. 5. χ vs T and ρ vs T for polycrystalline $BaFe_{2-x}Pt_xAs_2$ (HP). The χ was measured at $H = 10$ Oe.

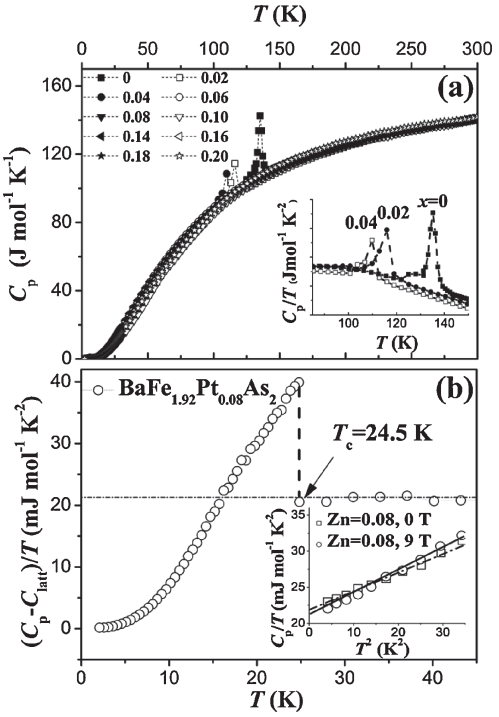

Fig. 6. (a) C_p vs T for polycrystalline $BaFe_{2-x}Pt_xAs_2$ (HP) with $x =$ 0.02–0.20. An expanded view close to the peaks at $x = 0$, 0.02, and 0.04 is shown in the inset. (b) $(C_p - C_{latt})/T$ vs T for $BaFe_{1.92}Pt_{0.08}As_2$. The inset shows C_p/T vs T^2 for $BaFe_{1.92}Zn_{0.08}As_2$ collected at 0 and 9 T for use as a lattice contribution reference.

Table I. Scale factors A and B, γ, and $N(E_F)$ of $BaFe_{2-x}Pt_xAs_2$.

x in $BaFe_{2-x}Pt_xAs_2$	A	B	γ (mJ mol^{-1} K^{-2})	$N(E_F)$ (states eV^{-1} f.u.$^{-1}$)
0.00	0.95	1.04	5.61	1.98
0.04	0.98	1.02	11.8	4.16
0.06	0.94	1.02	21.2	7.49
0.08	1.03	0.97	22.9	8.09
0.14	0.99	1.03	17.8	6.28
0.16	0.95	1.02	15.1	5.33
0.18	1.05	0.97	11.8	4.17
0.25	1.00	1.00	9.78	3.45

The C_p peak at T_c is often very broad in Fe-based superconductors. Thus, a careful subtraction of C_{latt} was essential to analyze the superconducting transition. In order to correctly subtract C_{latt} from the total C_p, we employed the C_p^{Zn} of the Zn-doped $BaFe_{1.92}Zn_{0.08}As_2$ as a reference because it shows neither SC nor SDW transitions.[28] The inset of Fig. 6(b) shows the C_p^{Zn}/T vs T^2 for $BaFe_{1.92}Zn_{0.08}As_2$. The small H dependence indicates insignificant magnetic factors in C_p^{Zn}. The Sommerfeld constant, γ^{Zn}, was estimated by fitting to a linear function ($C_p^{Zn} = \gamma^{Zn}T + \beta_{Zn}T^3$, where β_{Zn} is a coefficient), as shown. A γ^{Zn} of 22.1 mJ mol^{-1} K^{-2} was estimated. The C_{latt} of $BaFe_{2-x}Pt_xAs_2$ ($x = 0$–0.20) could then be calculated using the formula $C_{latt} = AC_p^{Zn}(BT) - \gamma^{Zn}T$, where A and B are variable parameters. The total C_p of $BaFe_{2-x}Pt_xAs_2$ ($x = 0$–0.20) then appears to fit well to the formula $C_p = C_{latt} + \gamma T$ between 40 and 130 K with a constraint regarding the entropy conservation. The refined values of the parameters used are summarized in Table I.

The specific heat jump at T_c of the optimally doped superconductor ($x = 0.08$) is plotted in Fig. 6(b) after the subtraction of C_{latt}. There is a sharp anomaly at 24.5 K (midpoint of the thermodynamical transition), which indicates T_c. In addition, the thermodynamical transition does occur close to T_c by ρ and χ. The specific heat jump, $\Delta C/\gamma T_c$, was ~1.55, which is slightly larger than the weak-coupling BCS limit of 1.43. The transition features suggest that the present compound was a strongly coupled superconductor.

In addition to the analysis of the SC jump, γ was roughly estimated by applying an extrapolation method above T_c: the largest γ of 22.9 mJ mol^{-1} K^{-2} was obtained at $x = 0.08$, which is within the expected range of 20–30 mJ mol^{-1} K^{-2} from a LDA+DMFT study.[29] This suggests that a large fraction of the Fermi surface was involved in the superconducting transition. The Pt doping led to an increase in γ from 5.61 mJ mol^{-1} K^{-2} ($x = 0$) to 22.9 mJ mol^{-1} K^{-2} ($x = 0.08$) in the under-doped region, while in the over-doped region, the doped Pt continuously decreased γ to 9.78 mJ mol^{-1} K^{-2} ($x = 0.25$). Note that analogous behaviors regarding γ have been observed for the other 122-type superconductors.[30,31] The quasi-particle density of states $N(E_F)$ for polarized spins can be calculated from the γ using the formula $\gamma = (1/3)\pi^2 k_B N(E_F)(1 + \lambda_{ef})$,[32] where λ_{ef} is the electron–phonon coupling constant. For the first approximation, λ_{ef} is set to 0, then $N(E_F)$ increases from 1.98 ($x = 0$) to 8.09 ($x = 0.08$) states eV^{-1} f.u.$^{-1}$, as shown in Table I, which suggests an appreciable increase in $N(E_F)$. Further Pt doping decreased $N(E_F)$ to 3.45 states eV^{-1} f.u.$^{-1}$ ($x = 0.20$). The estimated $N(E_F)$ systematically varied within the expected range in the theoretical calculations.[30]

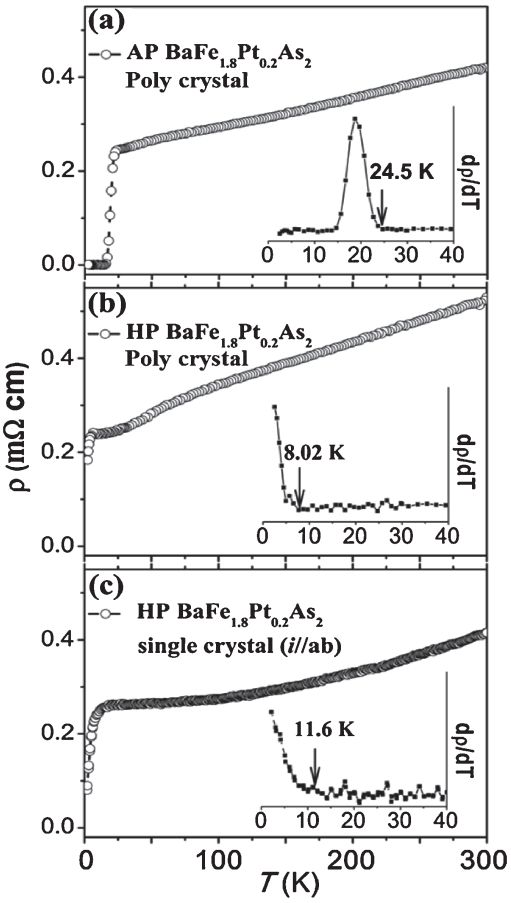

Fig. 7. Synthesis condition dependence of ρ vs T for $BaFe_{1.8}Pt_{0.2}As_2$: (a) AP polycrystalline pellet, (b) HP polycrystalline pellet, and (c) HP single crystal.

We next investigated the synthesis condition dependence of the ρ of $BaFe_{1.8}Pt_{0.2}As_2$. Figures 7(a)–7(c) show $\rho(T)$ curves for the AP- and HP-prepared polycrystals and a single crystal (HP) of $BaFe_{1.8}Pt_{0.2}As_2$. The AP sample shows a manifest drop at 24 K, while the HP samples (both the polycrystal and single crystal) show drops at much lower temperatures (8–12 K). It appears that the synthesis condition had a significant impact on the superconducting state. This motivated us to reinvestigate the superconducting phase diagram of $BaFe_{2-x}Pt_xAs_2$. The net Pt content of the AP sample should be somewhat overestimated because of the formation of a Pt rich impurity. Thus, the inhomogeneous distribution of Pt was most likely responsible for the significant T_c variation. However, the role of the $PtAs_2$ ingrowth has not been well explained in relation to the SC, but is left for a future work.

A revised phase diagram for $BaFe_{2-x}Pt_xAs_2$ is proposed in Fig. 8. The data were obtained solely from the HP-prepared samples. The revision is significant, especially in the over-doped area; the revised diagram no longer shows an unusually wide SC area with an almost invariable T_c, as indicated in early studies,[20] but rather a dome-like SC area. The optimal T_c was achieved using a Pt doping of 4 at. %, which was comparable to adding 0.08 extra electrons per Fe. This number is common to other 3*d* and 4*d* element doped $BaFe_{2-x}M_xAs_2$ superconductors.[33] In addition, the coex-

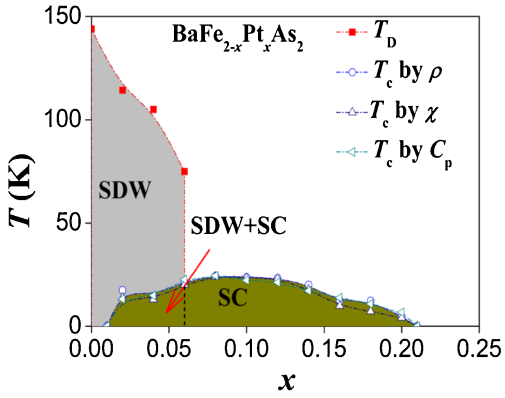

Fig. 8. (Color online) Revised T–x phase diagram for $BaFe_{2-x}Pt_xAs_2$.

istence of an AFM order and superconductivity was confirmed in the under-doped region ($x \leq 0.04$); further investigation of the coexistence is left for future work. In order to secure the present results, we carefully repeated the same experiment: the composition x was investigated more than two times by XRD and EDX using independently synthesized samples. We conclude that the present results are certainly reproducible.

Hereafter, we focus on the optimal SC of $BaFe_{2-x}Pt_xAs_2$. The isothermal magnetization of the polycrystalline $BaFe_{1.92}Pt_{0.08}As_2$ was measured, as presented in Fig. 9(a). The magnetic hysteresis loops at various temperatures were quite symmetric, suggesting a bulk pinning nature. The critical current density (J_c) at 2 K was estimated to be $\sim 2.8 \times 10^5$ A/cm^2 via the Bean model.[34] The J_c was nearly comparable to that for a single crystal of $BaFe_{1.92}Pt_{0.08}As_2$ (3.4×10^5 A/cm^2 at 2 K, our sample) as well as to the other J_c reported for doped 122-type superconductors ($\sim 10^5$–10^6 A/cm^2).[35,36] The result thus indicates that the polycrystalline nature of $BaFe_{2-x}Pt_xAs_2$ does not have a prominent impact on the SC. Note that a comparable conclusion was stated for the HP-prepared 1111-type superconductor.[37] The result could alternately indicate that the polycrystalline nature is not a major source of the revision of the phase diagram.

For further investigation of the optimal SC, the H dependence of the $\rho(T)$ of $BaFe_{1.92}Pt_{0.08}As_2$ was measured, as shown in Fig. 9(b). With an increase in the magnitude of the applied H, T_c steadily decreased. However, even in the highest magnetic field, the drop remained very sharp, suggesting that the upper critical field (H_{c2}) was very high, as reported elsewhere.[19,20] The $H_{c2}(T)$ plot against T in the inset to Fig. 9(b) roughly estimates $\mu_0 H_{c2}(0)$ to be 90 T, where μ_0 is the permeability constant, by an extrapolation method using the Werthamer–Helfand–Hohenberg relation $\mu_0 H_{c2}(0) = -0.693(\mathrm{d}H_{c2}/\mathrm{d}T)_{T=T_c} T_c$.[38] This estimation is slightly larger than that of a single crystal $BaFe_{1.9}Pt_{0.1}As_2$ (65 T).[19] The $H_{c2}(0)$ estimation allows us to measure the superconducting coherence length (ξ_{GL}) via the single-band Ginzburg–Landau relation, $\xi_{GL} = [\Phi_0/2\pi H_{c2}(0)]^{1/2}$, where Φ_0 is the flux quantum. The ξ_{GL} for $BaFe_{1.92}Pt_{0.08}As_2$ is roughly $\sim$25 Å, which is nearly comparable to that for $BaFe_{1.8}Co_{0.2}As_2$ ($\sim$30 Å).[39] The Ginzburg number, κ, is calculated to be 4.84×10^{-4} using the formula $\kappa = (\pi\lambda_0 k_B T_c \mu_0 / 2\xi_{GL}\Phi_0^2)^2$, where λ_0 is the London penetration depth ($\sim$200 nm)[37] and k_B is the Boltzmann constant. The

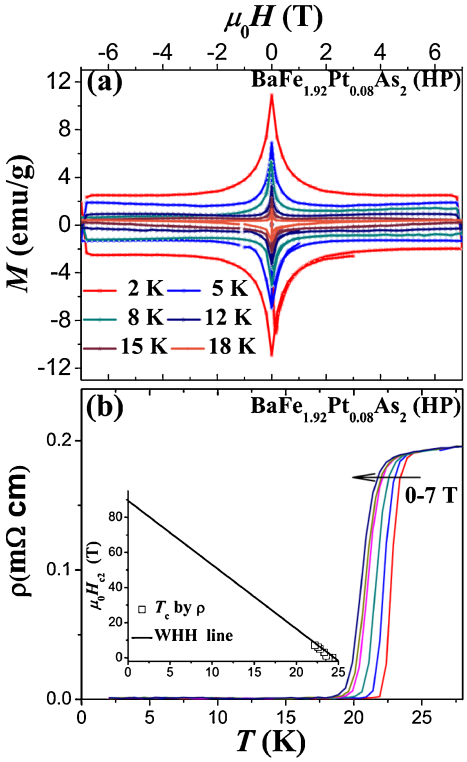

Fig. 9. (Color online) (a) Isothermal magnetization of optimal superconductor $BaFe_{1.92}Pt_{0.08}As_2$ (HP) measured at various temperatures. (b) Expanded view of the $\rho(T)$ measured for various magnitudes of $\mu_0 H$ (0, 0.1, 1, 3, 5, 6, and 7 T), and (inset) $\mu_0 H_{c2}$ vs T deduced from the ρ data.

relatively small ξ_{GL} and κ are good indications of strong coupling of the SC.

In the $s\pm$-wave model, the SC should be extremely sensitive to disorders.[40–43] However, the disorders associated with the doped Pt seem to have a minor impact on the SC, along with those by Co and Ni.[44] The small RRR for the present Pt-doped superconductor suggests that the impurity scatterings, including the disorder were substantial. However, the influence on the SC was weak. Recent impurity studies for 122-type superconductors found that even the strongest scattering center such as Zn does not decrease T_c as much as expected from the $s_\pm$-wave model, not only in the optimally doped but also in the under- and over-doped superconductors.[45,46] Although a 5d atom has an electronic state that is distinguishable from that of a 3d atom, the doped Pt seems to only play a role comparable to Ni and Co in the present Fe-based 122-type superconductor. Further theoretical studies for the impurity potential and band interactions of Pt in the conducting Fe_2As_2 layer are needed to reveal the role of the disorder associated with the dopant.

4. Conclusion

In summary, 5d atom doping to the AFM metallic compound $BaFe_2As_2$ was studied. A systematic doping control was successfully achieved using a HP method, and the SC properties were characterized using XRD, EDX, and by measuring ρ, χ, and C_p. The results confirmed the existence of a dome-like SC region for x values of 0.02 to 0.20 in the thermal phase diagram of $BaFe_{2-x}Pt_xAs_2$, as well as what was observed for the 3d and 4d doped $BaFe_2As_2$. The optimal T_c of 24.2 K ($x = 0.08$) was not far from the T_c

of the other doped $BaFe_2As_2$, which suggests that the electron–phonon coupling was insignificant. Note that an unusually wide SC area with an almost invariable T_c was not observed, unlike the findings of earlier studies, which suggest that an overestimation of the net Pt content might have complicated the earlier results. Clearly, further doping beyond the optimal Pt concentration continuously decreases T_c toward zero. The present result thus significantly revises the phase diagram proposed for $BaFe_{2-x}Pt_xAs_2$, suggesting a result resembling that of Pt-doped $SrFe_2As_2$ in which SC emerged in a comparable dome-like region with an optimal T_c of 16 K.[47] Additional studies of the role played by the disorders associated with Pt may further increase the optimal T_c of the 122-type superconductor.

Acknowledgments

We thank Dr. Miyakawa for the high-pressure experiments and Mr. Shirako for the EDX study. This research was supported in part by the World Premier International Research Center (WPI) Initiative on Materials Nanoarchitectonics from the Ministry of Education, Culture, Sports, Science and Technology, Japan; Grants-in-Aid for Scientific Research (22246083) from the Japan Society for the Promotion of Science (JSPS), Japan; and the Funding Program for World-Leading Innovative R&D on Science and Technology (FIRST Program) from JSPS.

1) Y. Kamihara, T. Watanabe, M. Hirano, and H. Hosono: J. Am. Chem. Soc. **130** (2008) 3296.
2) Z. A. Ren, W. Lu, J. Yang, W. Yi, X. L. Shen, Z. C. Li, G. C. Che, X. L. L. L. Sun, F. Zhou, and Z. X. Zhao: Chin. Phys. Lett. **25** (2008) 2215.
3) N. Ni, S. L. Bud'ko, A. Kreyssig, S. Nandi, G. E. Rustan, A. I. Goldman, S. Gupta, J. D. Corbett, A. Kracher, and P. C. Canfield: Phys. Rev. B **78** (2008) 014507.
4) M. Rotter, M. Tegel, D. Johrendt, I. Schellenberg, W. Hermes, and R. Pöttgen: Phys. Rev. B **78** (2008) 020503(R).
5) C. Krellner, N. Caroca-Canales, A. Jesche, H. Rosner, A. Ormeci, and C. Geibel: Phys. Rev. B **78** (2008) 100504(R).
6) Y. Xiao, Y. Su, M. Meven, R. Mittal, C. M. N. Kumar, T. Chatterji, S. Price, J. Persson, N. Kumar, S. K. Dhar, A. Thamizhavel, and T. Brueckel: Phys. Rev. B **80** (2009) 174424.
7) I. I. Mazin, D. J. Singh, M. D. Johannes, and M. H. Du: Phys. Rev. Lett. **101** (2008) 057003.
8) M. Rotter, M. Tegel, and D. Johrendt: Phys. Rev. Lett. **101** (2008) 107006.
9) A. S. Sefat, R. Jin, M. A. McGurie, B. C. Sales, D. J. Singh, and D. Mandrus: Phys. Rev. Lett. **101** (2008) 117004.
10) L. J. Li, Y. K. Luo, Q. B. Wang, H. Chen, Z. Ren, Q. Tao, Y. K. Li, X. Lin, M. He, Z. W. Zhu, G. H. Cao, and Z. A. Xu: New J. Phys. **11** (2009) 025008.
11) S. Sharma, A. Bharathi, S. Chandra, V. R. Reddy, S. Paulraj, A. T. Satya, V. S. Sastry, A. Gupta, and C. S. Sundar: Phys. Rev. B **81** (2010) 174512.
12) F. Han, X. Zhu, P. Chen, G. Mu, Y. Jia, L. Fang, Y. Wang, H. Luo, B. Zeng, B. Shen, L. Shan, C. Ren, and H. H. Wen: Phys. Rev. B **80** (2009) 024506.
13) Z. Bukowski, S. Weyeneth, R. Puzniak, P. Moll, S. Katrych, N. D. Zhigadlo, J. Karpinski, H. Keller, and B. Batlogg: Phys. Rev. B **79** (2009) 104521.
14) T. Sudayama, Y. Wakisaka, T. Mizokawa, S. Ibuka, R. Morinaga, T. J. Sato, M. Arita, H. Namatame, M. Taniguchi, and N. L. Saini: J. Phys. Soc. Jpn. **80** (2011) 113707.
15) H. Wadati, I. Elfimov, and G. A. Sawatzky: Phys. Rev. Lett. **105** (2010) 157004.
16) J. A. Wilson: J. Phys.: Condens. Matter **22** (2010) 203201.
17) M. M. Korshunov and I. Eremin: Phys. Rev. B **78** (2008) 140509.
18) T. Saito, S. Onari, and H. Kontani: Phys. Rev. B **82** (2010) 144510.
19) S. R. Saha, T. Drye, K. Kirshenbaum, N. P. Butch, and J. P. Paglione: J. Phys.: Condens. Matter **22** (2010) 072204.
20) X. Zhu, F. Han, G. Mu, P. Chen, J. Tang, J. Ju, K. Tanigaki, and H. H. Wen: Phys. Rev. B **81** (2010) 104525.
21) X. L. Wang, H. Y. Shi, X. W. Yan, Y. C. Yuan, Z. Y. Lu, X. Q. Wang, and T. S. Zhao: Appl. Phys. Lett. **96** (2010) 012507.
22) C. Dong: J. Appl. Crystallogr. **32** (1999) 838.
23) A. Czybulka, M. Noak, and H.-U. Schuster: Z. Anorg. Allg. Chem. **609** (1992) 122.
24) S. A. J. Kimber, A. Kreyssig, Y. Z. Zhang, H. O. Jeschke, R. Valenti, F. Yokaichiya, E. Colombier, J. Q. Yan, T. C. Hasen, T. Chatterji, R. J. McQueeney, P. C. Calfield, A. I. Goldman, and D. N. Argyriou: Nat. Mater. **8** (2009) 471.
25) J. Zhao, Q. Huang, C. de la Cruz, S. L. Li, J. W. Lynn, Y. Chen, M. A. Green, G. F. Chen, G. Li, Z. Li, J. L. Luo, N. L. Wang, and P. C. Dai: Nat. Mater. **7** (2008) 953.
26) N. Ni, A. Thaler, A. Kracher, J.-Q. Yan, S. L. Bud'ko, and P. C. Canfield: Phys. Rev. B **80** (2009) 024511.
27) C. de la Cruz, Q. Huang, J. W. Lynn, J. Li, W. Ratcliff II, J. L. Zarestky, H. A. Mook, G. F. Chen, J. L. Luo, N. L. Wang, and P. Dai: Nature **453** (2008) 899.
28) Y. F. Guo, J. J. Li, X. X. Wang, Y. Sun, C. Sathish, K. Yamaura, and E. Takayama-Muromachi: unpublished.
29) K. Haule, J. H. Shim, and G. Kotliar: Phys. Rev. Lett. **100** (2008) 226402.
30) K. Gofryk, A. S. Sefat, M. A. McGuire, B. C. Sales, D. Mandrus, J. D. Thompson, E. D. Bauer, and F. Ronning: Phys. Rev. B **81** (2010) 184518.
31) G. Mu, B. Zeng, P. Cheng, Z. S. Wang, L. Fang, B. Shen, L. Shan, C. Ren, and H. H. Wen: Chin. Phys. Lett. **27** (2010) 037402.
32) C. Kittel: *Introduction to Solid State Physics* (Wiley, New York, 1966) 4th ed.
33) A. S. Sefat, R. Jin, M. A. McGuire, B. C. Sales, D. J. Singh, and D. Mandrus: Phys. Rev. Lett. **101** (2008) 117004.
34) C. P. Bean: Rev. Mod. Phys. **36** (1964) 31.
35) S. Nandi, M. G. Kim, A. Kreyssig, R. M. Fernandes, D. K. Pratt, A. Thaler, N. Ni, S. L. Bud'ko, P. C. Canfield, J. Schmalian, R. J. McQueeney, and A. I. Goldman: Phys. Rev. Lett. **104** (2010) 057006.
36) N. Ni, M. E. Tillman, J.-Q. Yan, A. Kracher, S. T. Hannahs, S. L. Bud'ko, and P. C. Canfield: Phys. Rev. B **78** (2008) 214515.
37) M. Putti, I. Pallecchi, E. Bellingeri, M. R. Cimberle, M. Tropeano, C. Ferdeghini, A. Palenzona, C. Tarantini, A. Yamamoto, J. Jiang, J. Jaroszynski, F. Kametani, D. Abraimov, A. Polyanskii, J. D. Weiss, E. E. Hellstrom, A. Gurevich, D. C. Larbalestier, R. Jin, B. C. Sales, A. S. Sefat, M. A. McGuire, D. Mandrus, P. Cheng, Y. Jia, H. H. Wen, S. Lee, and C. B. Eom: Supercond. Sci. Technol. **23** (2010) 034003.
38) N. R. Werthamer, E. Helfand, and P. C. Hohenberg: Phys. Rev. **147** (1966) 295.
39) Y. Yin, M. Zech, T. L. Williams, X. F. Wang, G. Wu, X. H. Chen, and J. E. Hoffman: Phys. Rev. Lett. **102** (2009) 097002.
40) V. Cvetkovic and Z. Tesanovic: Europhys. Lett. **85** (2009) 37002.
41) S. Onari and H. Kontani: Phys. Rev. Lett. **103** (2009) 177001.
42) T. K. Ng: Phys. Rev. Lett. **103** (2009) 236402.
43) C. Tarantini, M. Putti, A. Gurenvich, Y. Shen, R. K. Singh, J. M. Rowell, N. Newman, D. C. Larbalestier, P. Cheng, Y. Jia, and H.-H. Wen: Phys. Rev. Lett. **104** (2010) 087002.
44) S. C. Lee, A. Kawabata, T. Moyoshi, Y. Kobayashi, and M. Sato: J. Phys. Soc. Jpn. **78** (2009) 043703; S. C. Lee, A. Kawabata, T. Moyoshi, Y. Kobayashi, and M. Sato: J. Phys. Soc. Jpn. **79** (2010) 023702.
45) J. J. Li, Y. F. Guo, S. B. Zhang, S. Yu, H. Kontani, Y. Tsujimoto, K. Yamaura, and E. Takayama-Muromachi: Phys. Rev. B **84** (2011) 020513(R).
46) J. Li, Y. Guo, S. Zhang, Y. Tsujimoto, X. Wang, C. I. Sathish, S. Yu, K. Yamaura, and E. Takayama-Muromachi: Solid State Commun. **152** (2012) 671.
47) K. Kirshenbaum, S. R. Saha, T. Drye, and J. Paglione: Phys. Rev. B **82** (2010) 144518.